Leakage Suppression in Pulse-Shaped OTFS Delay-Doppler-Pilot Channel Estimation

Andreas Pfadler, Tom Szollmann, Peter Jung, and Slawomir Stanczak, *Senior Member, IEEE*

***Abstract*—In this letter, we propose a novel channel estimation scheme with leakage suppression for orthogonal time frequency and space (OTFS) modulation. In OTFS, data and pilot symbols are placed in the delay-Doppler (DD) domain and spread over the time-frequency (TF) domain. This increases the achievable accuracy in estimating linear time-varying (LTV) channels. Unfortunately, leakage effects reduce the measurement precision significantly. Therefore, we propose a scheme that exploits smoothness regularization in TF to suppress the leakage observed in the DD domain. It allows us to improve the channel estimation accuracy while reducing signaling overhead.**

***Index Terms*—Delay-doppler, channel estimation, OTFS.**

I. Introduction

ONE OF the most promising features of orthogonal time frequency and space (OTFS) modulation is the direct resolution of the different channel paths in the DD domain. Therefore, it has the potential to provide more accurate channel estimation and reduced signaling overhead when using sparsity promoting estimation techniques like compressed sensing. This is particularly interesting for high-speed communication scenarios, involving, e.g., vehicle communications. Safety-relevant vehicle communications are especially challenging as they require a reliable exchange of short-frame messages. This implies that on the one hand, we have to meet strict quality of service requirements and, on the other hand, we need to deal with highly LTV channels. In these scenarios, the channel needs to be estimated and equalized on a per frame basis.

Considering the full OTFS transceiver chain, including pulse shaping filters, the original sparsity in the channel diminishes when using the discrete symplectic Fourier transform (DSFT). Depending on the LTV channel both fractional Doppler shifts and delay shifts are present when represented in the discrete DD domain. The reason for this is that the fractional shifts are not compatible with the periodicity assumption of the DSFT. This causes significant leakage and substantially reduces the effective sparsity.

So far, most research has focused on iterative detection methods based on message passing [1]–[3]. In [1] and [2], the channel is assumed to be sparse in the DD domain. Other works take fractional Doppler shifts but not fractional delay shifts into account [3], [4]. In [3], enlarged guard regions are used to deal with fractional Doppler shifts. In general, compressed sensing or even super resolution are possible approaches to cope with leakage effects and to enhance sparsity as presented in [5], [6], respectively. However, algorithms in this context usually require high computing power, are complex, and time-costly. This motivates a deeper investigation of low-complexity practical schemes to leakage suppression without resorting to ℓ_1-norm minimization or iterative optimization methods. A suitable scheme is channel main diagonal estimation (CMDE) with one-tap equalization [7], [8]. In this letter, we focus on CMDE with a novel smoothness regularization scheme that does not need the periodicity assumption to be fulfilled.

II. System Model

The system model for pulse-shaped multicarrier schemes is based on a time-continuous Gabor (Weyl-Heisenberg) signaling model from which we derive a discrete model. We define the Gabor grid as $\mathcal{I} \subseteq \mathbb{Z}_N \times \mathbb{Z}_M$ with $\mathbb{Z}_N = \{0, \dots, N-1\}$, $\mathbb{Z}_M = \{0, \dots, M-1\}$ and time- and frequency step-sizes $T > 0$ and $F > 0$, respectively. Note that we assume the grid to be cyclic. The frame duration is then the product of TN and total bandwidth $B = FM$. We further use $\mathcal{I}^\circ \subseteq \mathbb{Z}_M \times \mathbb{Z}_N$ to denote the adjoint grid corresponding to the DD domain. We synthesize the transmit signals $f_{\mathrm{Tx}}(t)$ with the pulse complex-valued pulse $\gamma(t)$ as

$$f_{\mathrm{Tx}}(t) \coloneqq \sum_{(n,m)\in\mathcal{I}} x_{n,m}\gamma(t-nT)\mathrm{e}^{2\pi jmFt}, \tag{1}$$

where $j = \sqrt{-1}$ and $\boldsymbol{x} = \{x_{n,m}\}_{(n,m)\in\mathcal{I}}$ is the 2D-array of TF-resource coefficients containing the TF spread symbols. The Gabor synthesis in (1) is also referred to as Heisenberg transform, as in [1]. All symbols $\boldsymbol{X} = \{X_{\ell,k}\}_{(\ell,k)\in\mathcal{I}^\circ}$ are placed in the DD and spread over the TF domain by applying the DSFT, i.e.,

$$x_{n,m} = [\mathcal{F}_{\mathrm{s}}X]_{n,m} \coloneqq \frac{1}{\sqrt{NM}} \sum_{(\ell,k)\in\mathcal{I}^\circ} X_{\ell,k}\, e^{-2\pi j(\frac{nk}{N}-\frac{m\ell}{M})}, \tag{2}$$

Manuscript received February 16, 2022; accepted March 10, 2022. Date of publication March 18, 2022; date of current version June 10, 2022. This work was supported by the Federal Ministry of Education and Research of Germany in the Programme of "Souverän. Digital. Vernetzt." Joint Project 6G-RIC under Project 16KISK020K. The associate editor coordinating the review of this article and approving it for publication was S. Sugiura. *(Corresponding author: Andreas Pfadler.)*

Andreas Pfadler is with the Autonomous Driving, Volkswagen Commercial Vehicles, 38436 Wolfsburg, Germany, and also with the Network and Information Theory, Technical University of Berlin, 10623 Berlin, Germany (e-mail: andreas.pfadler@volkswagen.de).

Tom Szollmann is with the Wireless Communications and Networks, Fraunhofer Heinrich Hertz Institute, 10587 Berlin, Germany (e-mail: tom.szollmann@hhi.fraunhofer.de).

Peter Jung is with the Wireless Communications and Networks, Fraunhofer Heinrich Hertz Institute, 10587 Berlin, Germany, and also with the Communications and Information Theory, Technical University of Berlin, 10623 Berlin, Germany (e-mail: peter.jung@hhi.fraunhofer.de).

Slawomir Stanczak is with the Wireless Communications and Networks, Fraunhofer Heinrich Hertz Institute, 10587 Berlin, Germany, and also with the Network and Information Theory, Technical University of Berlin, 10623 Berlin, Germany (e-mail: slawomir.stanczak@hhi.fraunhofer.de).

Digital Object Identifier 10.1109/LWC.2022.3160657

where $\mathcal{F}_{\mathrm{s}}$ denotes the DSFT and is also called OTFS transform. Note that $\mathcal{F}_{\mathrm{s}}$ is its own inverse due to the flipping of the axes, opposite exponential sign, and normalization.[1]

Assuming a LTV channel, the signal at the receiver yields

$$f_{\mathrm{Rx}}(t) \coloneqq \sum_{p\in\mathcal{J}} \eta_p f_{\mathrm{Tx}}(t-\tau_p)\mathrm{e}^{2\pi j\nu_p t}, \tag{3}$$

where f_{Tx} is given by (1) and $\mathcal{J}=\{1,\dots,P\}$ is the index set corresponding to the complex-valued channel coefficients η_p, delay shift τ_p and Doppler shift ν_p associated with each transmission path. The channel is assumed to be underspread, i.e., all tuples (τ_p,ν_p) are contained within a small box $\mathcal{U}\subset[0,\tau_{\max}]\times[-\nu_{\max},\nu_{\max}]$ of size $|\mathcal{U}|=2\tau_{\max}\nu_{\max}\ll 1$, where $\nu_{\max}$ and $\tau_{\max}$ denote the largest Doppler spread and delay spread, respectively [9]. At the Gabor filter bank, the received signal is measured with the complex-valued analysis pulse $g(t)$, i.e., the $(\bar{n},\bar{m})$-th measurement is

$$\begin{aligned} y_{\bar{n},\bar{m}} &= \int g^*(t-\bar{n}\,T)\mathrm{e}^{-2\pi j\bar{m}Ft} f_{\mathrm{Rx}}(t)\,\mathrm{d}\,t + w_{\bar{n},\bar{m}},\\ &= \sum_{p\in\mathcal{J}}\eta_p \underbrace{\int g^*(t-\bar{n}\,T)\mathrm{e}^{2\pi jt(\nu_p-\bar{m}F)} f_{\mathrm{Tx}}(t-\tau_p)\,\mathrm{d}\,t}_{=:y_{\bar{n},\bar{m}}(\tau_p,\nu_p)} + w_{\bar{n},\bar{m}}, \end{aligned} \tag{4}$$

where $(\cdot)^*$ denotes the complex conjugate and $\boldsymbol{y}(\tau,\nu)=\{y_{n,m}(\tau,\nu)\}_{(n,m)\in\mathcal{I}}$ is the 2D-array receiver response to a single unit amplitude scatterer with delay shift τ and Doppler shift ν. The Gabor analysis in (4) is also called Wigner transform, as in [1]. For the measurement error $\boldsymbol{w}=\{w_{\bar{n},\bar{m}}\}_{(\bar{n},\bar{m})\in\mathcal{I}}$, we assume an additive white Gaussian noise (AWGN) process, i.e., $w_{\bar{n},\bar{m}}\sim\mathcal{N}(0,\sigma^2)$. The assumption of white noise is common when using orthogonal receive filterbanks [10].

The unit response further evaluates to

$$\begin{aligned} y_{\bar{n},\bar{m}}(\tau,\nu) &= \sum_{(n,m)\in\mathcal{I}} x_{n,m}\\ &\times \int g^*(t-\bar{n}\,T)\gamma(t-\tau-nT)\mathrm{e}^{2\pi j(t\nu-\bar{m}Ft+mFt-mF\tau)}\,\mathrm{d}\,t \end{aligned} \tag{5}$$

and the integral in (5) is the full channel matrix given by

$$\mathrm{e}^{2\pi j(\bar{n}\,T\nu-mF\tau+TF\bar{n}\Delta m)}\int g^*(t)\gamma(t-\tau-\Delta nT)\mathrm{e}^{2\pi jt(\nu+\Delta mF)}\,\mathrm{d}\,t, \tag{6}$$

where we use $\Delta n=n-\bar{n}$ and $\Delta m=m-\bar{m}$ for convenience. The integral in (6) is the *cross ambiguity function* defined as $A_{\gamma,g}(\tau,\nu)\coloneqq\int g(t)^*\gamma(t-\tau)e^{2\pi j\nu t}dt$. Due to the underspread assumption, the channel matrix is diagonally dominant and most energy is contained in the channel main diagonal [11], which motivates the use of CMDE. Assuming a CMDE scheme, we separate the off-diagonal terms in (5) which correspond to self-interference in common terminology [11]. Self-interference includes both, inter-symbol and inter-carrier interference and is also referred to as channel cross-talk [8], [11]. We write the self-interference associated with a single unit amplitude scatterer as

$$\begin{aligned} z_{\bar{n},\bar{m}}(\tau,\nu) \coloneqq \sum_{\substack{(n,m)\in\mathcal{I}\\(n,m)\neq(\bar{n},\bar{m})}} & x_{n,m}\mathrm{e}^{-2\pi j(mF\tau-\bar{n}\,T\nu-TF\bar{n}\Delta m)}\\ &\times A_{\gamma,g}(\tau+T\Delta n,\nu+F\Delta m). \end{aligned} \tag{7}$$

Then, we can write (5) as

$$y_{\bar{n},\bar{m}}(\tau,\nu)=x_{\bar{n},\bar{m}}\underbrace{\mathrm{e}^{-2\pi j(\bar{m}F\tau-\bar{n}\,T\nu)}A_{\gamma,g}(\tau,\nu)}_{=:h_{\bar{n},\bar{m}}(\tau,\nu)}+z_{\bar{n},\bar{m}}(\tau,\nu), \tag{8}$$

where the 2D-array $\boldsymbol{h}(\tau,\nu)=\{h_{\bar{n},\bar{m}}(\tau,\nu)\}_{(\bar{n},\bar{m})\in\mathcal{I}}$ contains the channel main diagonal coefficients with respect to a single unit scatterer. Finally, this yields the input-output relation

$$\boldsymbol{y}=\boldsymbol{x}\odot\underbrace{\sum_{p\in\mathcal{J}}\eta_p\boldsymbol{h}(\tau_p,\nu_p)}_{=:\boldsymbol{h}}+\underbrace{\sum_{p\in\mathcal{J}}\boldsymbol{\eta}_p\boldsymbol{z}(\tau_p,\nu_p)}_{=:\boldsymbol{z}}+\boldsymbol{w}, \tag{9}$$

where $\boldsymbol{h}=\{h_{\bar{n},\bar{m}}\}_{(\bar{n},\bar{m})\in\mathcal{I}}$ is the 2D-array of the channel main diagonal, $\boldsymbol{z}=\{z_{\bar{n},\bar{m}}\}_{(\bar{n},\bar{m})\in\mathcal{I}}$ is the 2D-array of the self-interference, and $\odot$ denotes the *Hadamard product*. Applying the DSFT to (9), we transfer the relation to the DD domain

$$\begin{aligned} \boldsymbol{Y} &= \boldsymbol{X}\circledast\sum_{p\in\mathcal{J}}\eta_p\boldsymbol{H}(\tau_p,\nu_p)+\boldsymbol{Z}+\boldsymbol{W}, &(10)\\ &= \boldsymbol{X}\circledast\boldsymbol{H}+\boldsymbol{Z}+\boldsymbol{W}, &(11) \end{aligned}$$

where $[\boldsymbol{X}\circledast\boldsymbol{H}]_{\bar{\ell},\bar{k}}\coloneqq\sum_{m,n}X_{m,n}H_{\bar{\ell}-m,\bar{k}-n}$ denotes the 2D circular convolution of 2D-arrays. In the DD domain, $\boldsymbol{H}$, $\boldsymbol{Z}$, and $\boldsymbol{W}$ are 2D-arrays of the channel main diagonal, the self-interference, and AWGN, respectively. Note that $\boldsymbol{Z}$ includes both inter-Doppler and inter-delay interference. It is common to assume that the synthesis pulse γ, analysis pulse g, as well as T and F are adapted to $\mathcal{U}$ such that the self-interference is minimized [7], [8], i.e., $\|\boldsymbol{Z}\|_2^2\ll\|\boldsymbol{X}\circledast\boldsymbol{H}\|_2^2$. We model the distribution of $\boldsymbol{Z}$ as an additive white noise process $Z_{\bar{\ell},\bar{k}}\sim\mathcal{N}(0,\sigma_z^2)$ with (unknown) variance $\sigma_z^2>0$ which we regard as additional noise [8]. In (11), the channel represents a 2D convolution of 2D-arrays due to using the DSFT. Since the channel is considered to be underspread, we know that the 2D convolution kernel is supported within a region in the DD domain which we refer to as *pilot region* in Section IV. Therefore, standard CMDE yields the estimate $\hat{\boldsymbol{h}}$ by extracting this kernel from $\boldsymbol{Y}$. For equalization, we can then use a one-tap minimum mean square error equalizer (MMSE) and get the equalized frame as [8]

$$\hat{x}_{n,m}=\hat{h}_{n,m}^*y_{n,m}(|\hat{h}_{n,m}|^2+\lambda)^{-1}, \tag{12}$$

where $\lambda>0$ is the noise variance parameter.

III. Leakage Effect on Discrete DD Channel

Computing the channel coefficients for a (τ,ν)-scatterer in DD domain yields

$$H_{\bar{\ell},\bar{k}}(\tau,\nu)=\sum_{(\bar{n},\bar{m})\in\mathcal{I}}h_{\bar{n},\bar{m}}(\tau,\nu)\,\mathrm{e}^{-2\pi j(\frac{\bar{m}\bar{\ell}}{M}-\frac{\bar{n}\bar{k}}{N})}, \tag{13}$$

[1]LTFAT http://ltfat.org/doc/gabor/dsft.html

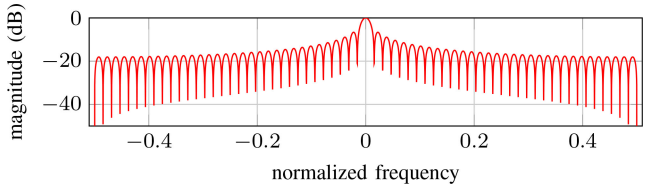

Fig. 1. Dirichlet kernel in spectrum (K = 64).

$$= A_{\gamma,g}(\tau,\nu) \sum_{\bar{n}=0}^{N-1} \mathrm{e}^{2\pi j \frac{\bar{n}(\bar{k}+NT\nu)}{N}} \sum_{\bar{m}=0}^{M-1} \mathrm{e}^{-2\pi j \frac{\bar{m}(\bar{\ell}+MF\tau)}{M}}, \quad (14)$$

$$= A_{\gamma,g}(\tau,\nu) D_N\left(\frac{\bar{k}+NT\nu}{N}\right) D_M\left(\frac{-\bar{\ell}-MF\tau}{M}\right), \quad (15)$$

where D_K is the *Dirichlet kernel* for an integer $K > 0$ defined to be

$$D_K(t) := \sum_{k=0}^{K-1} \mathrm{e}^{2\pi jkt} = \mathrm{e}^{\pi j(K-1)t} \frac{\sin(\pi Kt)}{\sin(\pi t)}. \quad (16)$$

Note that the length and bandwidth of the bi-orthogonal synthesis and analysis pulses are designed to be proportional to the spacing of the Gabor grid. In combination with the underspread assumption, we observe that $A_{g,\gamma}(\tau_p,\nu_p) \approx A_{g,\gamma}(0,0) = 1$ [11]. Consequently, the impact of the cross ambiguity function on the observed leakage in (15) is small. Fig. 1 illustrates the decay of the *Dirichlet kernel* for $K = 64$. Observe that the 2D-array $\boldsymbol{H}(\tau,\nu)$ is only sparse if $MF\tau$ and $NT\nu$ are both integers. Otherwise, it has many large entries due to the poor localization of the Dirichlet kernel, as shown in Fig. 1, which is commonly referred to as *leakage*.

Recall that the implicit assumption behind the DSFT is that the underlying samples stem from a band-limited periodic function, which is the reason for using a (block) cyclic prefix. However, $\boldsymbol{h}(\tau,\nu)$ is not cyclic and therefore the received frame $\boldsymbol{y}$ is discontinuous at the boundaries when interpreted as a periodic function. This behavior can be seen when comparing the frame borders of perfect with standard CMDE in Fig. 4(a) and 4(e), respectively. It can be observed that the standard CMDE reconstructs a periodic 2D-array in the TF domain, i.e., $\boldsymbol{h}$. In addition, the extraction of the pilot region applied in the DD domain acts upon $\boldsymbol{y}$ as an ideal low-pass filter, which is known to cause significant oscillations near discontinuities. This behavior is clearly visible for standard CMDE in Fig. 4(e).

IV. Structure of the OTFS Frame

All symbols are placed in the DD domain including the pilot signaling. We divide the frame into three regions, which are allocated according to the expected long-term expectation of the channel described by $\mathcal{U}$ [3]. The regions are specified by Q in Doppler domain and W and W_n both in delay domain and are depicted in Fig. 2. Unlike Doppler shifts, delays are distributed asymmetrically, i.e., with sufficient synchronization effective delays are usually non-negative. However, leakage smears delays such that we can also observe negative delays which can not be taken into accounted by W. Therefore, we introduce the parameter W_n. Doppler shifts are distributed

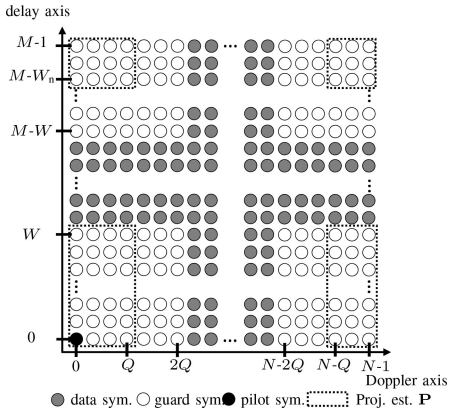

Fig. 2. OTFS frame with $W = 10$, $Q = 3$, and $W_\mathrm{n} = 3$.

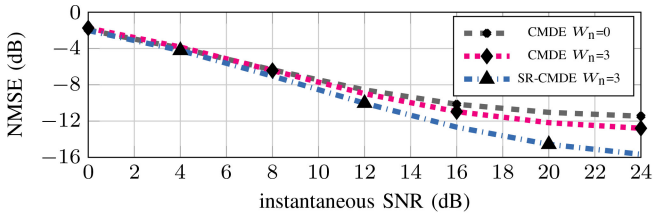

(a) Channel estimation error compared to perfect CMDE

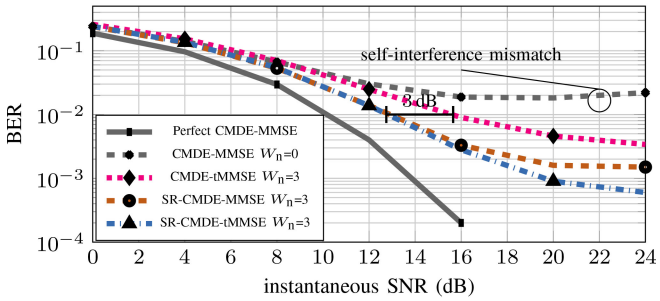

(b) Uncode bit error rate (BER)

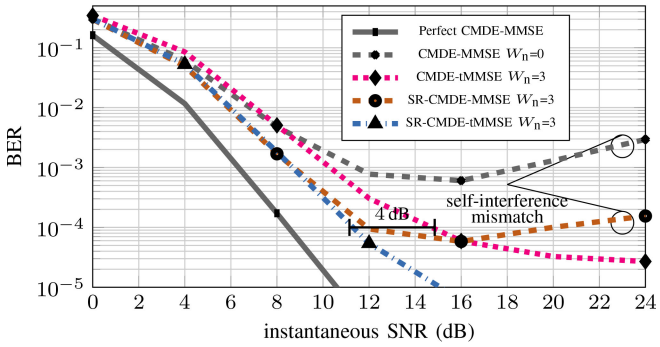

(c) Coded BER (convolutional hard-decision decoding, rate $r = 1/3$)

Fig. 3. Performance of CMDE and one-tap equalization in a NLOS vehicular scenario at $\Delta v = 200\,\mathrm{km/h}$.

symmetrically and we consider the smeared Doppler shifts by simply increasing Q. Recall that we have cyclic indices and therefore negative indices are wrapped.

1) *Pilot Region:* This region is a rectangular box given by

$$\mathcal{I}_\mathrm{p} = \{-Q,\ldots,Q\} \times \{-W_\mathrm{n},\ldots,W\} \subset \mathcal{I}^\circ \quad (17)$$

and consists of a single pilot symbol at the origin, i.e., $X_{0,0} = \sqrt{(4Q+1)(2W+1)}$ and zeros elsewhere.

The reasoning is that the main diagonal acts as a 2D-convolution with a kernel of approximate support size $(W + W_{\mathrm{n}} + 1) \times (2Q + 1)$, where W and Q are selected to be larger than the expected $\tau_{\max}MF$ and $\nu_{\max}NT$, respectively. The kernel of the channel main diagonal can be extracted using the orthogonal coordinate projection $\mathbf{P} \in \mathbb{C}^{MN \times M\bar{N}}$ onto the coordinates in $\mathcal{I}_{\mathrm{p}}$. $\mathbf{P}$ is the diagonal matrix with entries $[\mathbf{P}]_{(\bar{\ell},\bar{k}),(\bar{\ell},\bar{k})} = 1$ if $(\bar{l},\bar{k}) \in \mathcal{I}_{\mathrm{p}}$ and $[\mathbf{P}]_{(\bar{\ell},\bar{k}),(\bar{\ell},\bar{k})} = 0$ otherwise. Fig. 2 shows the projection $\mathbf{P}$ highlighted in a black dashed frame.

2) *Guard Region:* The *guard region*

$$\mathcal{I}_{\mathrm{g}} = (\{-2Q, \ldots, 2Q\} \times \{-W, \ldots, W\}) \backslash \mathcal{I}_{\mathrm{p}}, \quad (18)$$

consists entirely of zeros and avoids interference between pilot and data symbols outside the black dashed frame.

3) *Data Region:* All remaining symbols $\mathcal{I}_{\mathrm{d}} = \mathcal{I}^{\circ} \backslash (\mathcal{I}_{\mathrm{p}} \cup \mathcal{I}_{\mathrm{g}})$, usually coming from a certain modulation alphabet, are used for the data payload and have unit amplitude.

V. Channel Estimation and Smoothness Regularization

We propose a novel scheme to suppress the leakage effect for CMDE. The leakage is an inherent problem of the DSFT and is unavoidable if the pilot is subject to OTFS spreading. To mitigate this effect, we propose to combine a standard CMDE with additional minimization of the isotropic discrete gradients of $\boldsymbol{h}$, which we abbreviate as smoothness regularized channel main diagonal estimation (SR-CMDE).

Define the discrete gradient matrices $\Delta_{\mathrm{t}}, \Delta_{\mathrm{f}} \in \mathbb{C}^{NM \times NM}$ with mirror padding to be

$$[\Delta_{\mathrm{t}} h]_{\bar{n},\bar{m}} \coloneqq \begin{cases} h_{\bar{n}+1,\bar{m}} - h_{\bar{n},\bar{m}}, & \bar{n} = 0, \ldots, N-2, \\ 0, & \bar{n} = N-1, \end{cases} \quad (19)$$

and

$$[\Delta_{\mathrm{f}} h]_{\bar{n},\bar{m}} \coloneqq \begin{cases} h_{\bar{n},\bar{m}+1} - h_{\bar{n},\bar{m}}, & \bar{m} = 0, \ldots . M-2, \\ 0, & \bar{m} = M-1. \end{cases} \quad (20)$$

With this in hand, we consider the following optimization problem

$$\min_{\boldsymbol{h} \in \mathbb{C}^{NM}} \tfrac{1}{2} \|\mathbf{P}\mathcal{F}_{\mathrm{s}}\boldsymbol{h} - \hat{\boldsymbol{H}}\|_2^2 + \tfrac{\alpha}{2}(\|\Delta_{\mathrm{t}}\boldsymbol{h}\|_2^2 + \|\Delta_{\mathrm{f}}\boldsymbol{h}\|_2^2), \quad (21)$$

where the left term is a standard least-squares CMDE and the right term suppresses leakage. The regularization parameter $\alpha > 0$ has to be tuned for particular scenarios. Problem (21) can be solved by standard least-squares algorithms and has a closed form solution. Let us define

$$\boldsymbol{\Phi}_{\alpha} \coloneqq \begin{bmatrix} (\mathbf{P}\mathcal{F}_{\mathrm{s}})^{\mathsf{T}} & \sqrt{\alpha}\Delta_{\mathrm{t}}^{\mathsf{T}} & \sqrt{\alpha}\Delta_{\mathrm{f}}^{\mathsf{T}} \end{bmatrix}^{\mathsf{T}} \in \mathbb{C}^{3NM \times NM}, \quad (22)$$

$$\boldsymbol{\Phi} \coloneqq \begin{bmatrix} \hat{\boldsymbol{H}}^{\mathsf{T}} & \mathbf{0}_{NM}^{\mathsf{T}} & \mathbf{0}_{NM}^{\mathsf{T}} \end{bmatrix}^{\mathsf{T}} \in \mathbb{C}^{3NM}, \quad (23)$$

where $(\cdot)^{\mathsf{T}}$ is the transpose and $\mathbf{0}_{NM} \in \mathbb{C}^{NM}$ a zero 2D-array. Then, (21) is equivalent to

$$\min_{\boldsymbol{h} \in \mathbb{C}^{NM}} \tfrac{1}{2} \|\boldsymbol{\Phi}_{\alpha}\boldsymbol{h} - \boldsymbol{\Phi}\|_2^2, \quad (24)$$

TABLE I
Simulation and System Parameters

Parameter	Notation	Values
Carrier frequency	f_c	5.9 GHz
Bandwidth	B	5 MHz
Time/Doppler symbols	N	64
Frequency/delay symbols	M	64
Guards delay domain	W	10
Guards Doppler domain	Q	3
Signaling overhead	$(4Q+1)(2W+1)$	273
Modulation scheme	QPSK	-
Time-frequency product	TF	1.25
Synthesize and analysis pulse	γ and y	orthogonalized Gaussian-like
Channel model	QuaDRIGa v2.4.0 3GPP 38.901 UMi NLOS [12]	-

which has the unique solution $\boldsymbol{\Phi}_{\alpha}^{\dagger}\boldsymbol{\Phi}$, where $\boldsymbol{\Phi}_{\alpha}^{\dagger}$ is the *Moore-Penrose pseudo-inverse* of $\boldsymbol{\Phi}_{\alpha}$. Note that the matrix $\boldsymbol{\Phi}_{\alpha}^{\dagger}$ can be computed ahead of time so that (21) is solved by a single matrix-vector product.

VI. Numerical Results

We numerically study distinct schemes for CMDE together with one-tap equalization in vehicular scenarios where the channel is highly time-variant. We compare standard CMDE with the proposed SR-CMDE. The CMDE of the LTV channel is then used for one-tap equalization to evaluate the bit error rate (BER) performance. We consider two kinds of equalizers: (i) standard MMSE; (ii) tuned MMSE (tMMSE) with an extended variance parameter λ [7]. The latter one amounts for the self-interference and channel estimation error power in (12) as additional noise [8].

We use short-frame vehicular messages with 64 elements in both delay and Doppler domain, resulting in 4096 symbols in total. The *guard region* is selected to be $W = 10$ and $Q = 3$ yielding 3823 data and 273 signaling symbols and a signaling overhead of 6.67%. The larger the frames are, the lower the signaling overhead gets. This should be taken into account when comparing efficiency in terms of signaling overhead. The simulation and system parameter setup are listed in Table I. We focus on particular challenging non-line-of-sight (NLOS) vehicular scenarios with a relative velocity of $\Delta v = 200\,\mathrm{km/h}$, causing a large spreading region of $|U| = 4.25\text{e-}3$. The numerical system model takes fractional delay shifts and fractional Doppler shifts into account, reproducing leakage as observed in real measurements. Fig. 3a shows the normalized mean square error (NMSE) of the CMDE, where the best performance is achieved by the proposed SR-CMDE. In Fig. 3b, the uncoded BER performance is compared. In the case of standard MMSE, without tuning, the self-interference power dominates over the noise power for higher signal-to-noise-ratio (SNR) increasing the BER. Note that a more appropriate time-step T, frequency-step F, and pulse width may lead to better performance gains in terms of BER by improving the pulse and grid matching [10], [13]. Improvements of more than 3 dB are possible with target error rates below 1e-2. Fig. 3c shows the coded BER performance using convolutional code with a code rate of $r = 1/3$ with hard decision decoding. Here, improvements of 4 dB are possible with a target BER of 1e-4. From the numerical results it can be seen that the proposed SR-CMDE together with tMMSE enables a low complexity and robust communication.

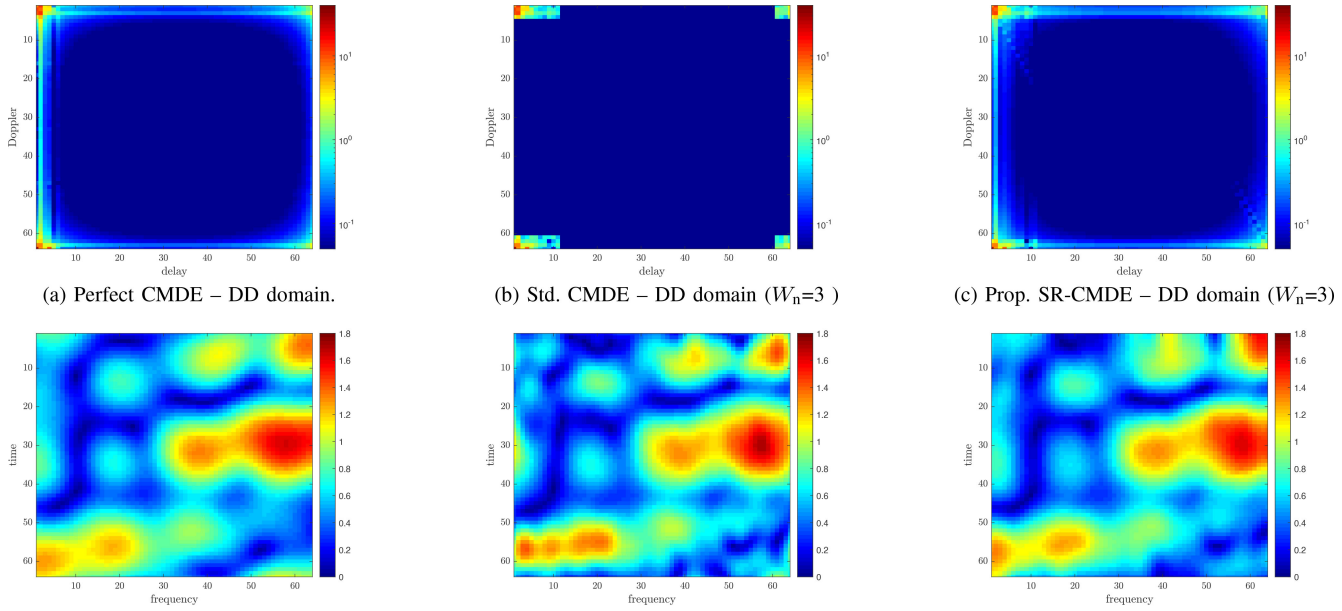

(a) Perfect CMDE – DD domain. (b) Std. CMDE – DD domain (W_{n}=3) (c) Prop. SR-CMDE – DD domain (W_{n}=3)

(d) Perfect CMDE – TF domain. (e) Std. CMDE – TF domain (W_{n}=3) (f) Prop. SR-CMDE – TF domain (W_{n}=3)

Fig. 4. CMDE for a particular NLOS vehicular channel realization at $\Delta v = 200\,\mathrm{km/h}$. Note that a less variant channel is selected, such that oscillations due to low-pass filtering are visible in (d) – other channel realizations are significantly more variant.

VII. Conclusion

We addressed the problem of leakage effects for pulse-shaped OTFS channel estimation. Leakage is caused by fractional delay and fractional Doppler shifts. To mitigate this effect, we proposed a novel minimization of the isotropic discrete gradients in the TF domain and combine it with standard channel main diagonal estimation. The numerical results indicate that the proposed scheme enables channel estimation with reduced signaling overhead even in highly time-variant communication scenarios. It was shown that the BER can be improved by more than 3-4 dB.

References

[1] M. K. Ramachandran and A. Chockalingam, "MIMO-OTFS in high-doppler fading channels: Signal detection and channel estimation," in *Proc. IEEE Global Commun. Conf. (GLOBECOM)*, Dec. 2018, pp. 206–212.

[2] K. R. Murali and A. Chockalingam, "On OTFS modulation for high-doppler fading channels," in *Proc. Inf. Theory Appl. Workshop (ITA)*, 2018, pp. 1–10.

[3] P. Raviteja, K. T. Phan, and Y. Hong, "Embedded pilot-aided channel estimation for OTFS in delay-doppler channels," *IEEE Trans. Veh. Technol.*, vol. 68, no. 5, pp. 4906–4917, May 2019.

[4] Z. Wei, W. Yuan, S. Li, J. Yuan, and D. W. K. Ng, "Transmitter and receiver window designs for orthogonal time-frequency space modulation," *IEEE Trans. Commun.*, vol. 69, no. 4, pp. 2207–2223, Apr. 2021.

[5] G. Taubock, F. Hlawatsch, D. Eiwen, and H. Rauhut, "Compressive estimation of doubly selective channels in multicarrier systems: Leakage effects and sparsity-enhancing processing," *IEEE J. Sel. Topics Signal Process.*, vol. 4, no. 2, pp. 255–271, Apr. 2010.

[6] R. Beinert, P. Jung, G. Steidl, and T. Szollmann, "Super-resolution for doubly-dispersive channel estimation," *Sampling Theory Signal Process. Data Anal.*, vol. 19, no. 2, p. 16, 2021.

[7] A. Pfadler, P. Jung, and S. Stanczak, "Pulse-shaped OTFS for V2X short-frame communication with tuned one-tap equalization," in *Proc. (WSA) 24rd Int. ITG Workshop Smart Antennas*, 2020, pp. 1–6.

[8] A. Pfadler, P. Jung, T. Szollmann, and S. Stanczak, "Pulse-shaped OTFS over doubly-dispersive channels: One-tap vs. full LMMSE equalizers," in *Proc. IEEE Int. Conf. Commun. Workshops (ICC Workshops)*, 2021, pp. 1–6.

[9] P. Bello, "Characterization of randomly time-variant linear channels," *IEEE Trans. Commun. Syst.*, vol. 11, no. 4, pp. 360–393, Dec. 1963.

[10] P. Jung and G. Wunder, "WSSUS pulse design problem in multicarrier transmission," *IEEE Trans. Commun.*, vol. 55, no. 9, p. 1822, Sep. 2007.

[11] F. Hlawatsch and G. Matz, *Wireless Communications Over Rapidly Time-Varying Channels*. Cambridge, MA, USA: Academic Press, 2011.

[12] S. Jaeckel, L. Raschkowski, K. B˝orner, and L. Thiele, "QuaDRiGa: A 3-D multi-cell channel model with time evolution for enabling virtual field trials," *IEEE Trans. Antennas Propag.*, vol. 62, no. 6, pp. 3242–3256, Jun. 2014.

[13] A. Pfadler, P. Jung, and S. Stanczak, "Mobility modes for pulse-shaped OTFS with linear equalizer," in *Proc. (GLOBECOM) IEEE Global Commun. Conf.*, 2020, pp. 1–6.